




Dielectric, electric, and piezoelectric properties of three-phase piezoelectric composite based on castor-oil polyurethane, lead zirconate titanate particles and multiwall carbon nanotubes

Fernando C. M. Freire Filho¹ | Josiane A. Santos¹ | Alex O. Sanches¹  |
Eliton S. Medeiros²  | José A. Malmonge¹  | Michael J. Silva³ 

¹Faculdade de Engenharia, Universidade Estadual Paulista (UNESP), Ilha Solteira, Brazil

²Laboratory of Materials and Biosystems (LAMAB), Universidade Federal da Paraíba (UFPB), Departamento de Engenharia de Materiais, João Pessoa, Brazil

³Faculdade de Engenharia e Ciência, Universidade Estadual Paulista (UNESP), Rosana, Brazil

Correspondence

Michael J. Silva, Faculdade de Engenharia e Ciência, Universidade Estadual Paulista (UNESP), Campus de Rosana, Rosana, SP, Brazil.

Email: michael.silva@unesp.br

Funding information

Sao Paulo State Funding Agency (FAPESP), Grant/Award Number: 2017/19809-5; CEPID - CDMF, Grant/Award Number: 2013/07296-2; Conselho Nacional de Desenvolvimento Científico e Tecnológico-CNPq, Grant/Award Number: 158889/2019-2

Abstract

The effects of multiwall carbon nanotubes (MWCNTs) on the electrical, dielectric, and piezoelectric properties of the ferroelectric ceramic/castor-oil polyurethane (PUR) composite films were evaluated. The three-phase piezoelectric composites were produced by keeping PUR concentration constant while varying lead zirconate titanate (PZT) volume fractions between 10 and 50 vol.%, at two MWCNT concentrations: above and below percolation threshold. The *dc* electrical conductivity analysis revealed that small amounts of MWCNTs dispersed within PUR/PZT composite films can significantly improve electrical and piezoelectric properties due to their ability to act as conductive bridges between PZT particles in the samples. Using Jonscher's power law, it was possible to determine that the electrical conduction in *ac* regime occurs through spatial charge hopping between states located within the piezoelectric composite. Analyzing the piezoelectric properties through the d_{33} coefficient, it was found that PUR-MWCNT/PZT piezoelectric composite displayed higher d_{33} values (20 pC/N) in comparison to the PUR/PZT two-phase composite (9.5 pC/N) for all PZT loadings. According to these results, the dispersion of MWCNT nanoparticles influences the poling effectiveness of the PZT particles and increases the d_{33} coefficient of three-phase piezoelectric composites.

KEYWORDS

castor-oil polyurethane, composite, multiwalled carbon nanotubes, piezoelectricity, lead zirconate titanate

1 | INTRODUCTION

Composites materials are defined as materials formed from at least two different components with distinct properties, whose inherent properties are combined to make a new material.^{1–3} Composites have thus distinguished themselves as a viable alternative to

conventional or single-phase materials, because of their wide range of applications such as in automotive industry, aeronautics, electro-electronics, and biomedicine.^{4,5}

There are several types of composites that can be studied, including those formed by a polymer matrix as the first phase and organic or inorganic particles as the second phase, including carbon-based nanoparticles

(carbon black (CB), graphene, carbon nanotube (CNT)), natural and synthetic fibers, ferroelectric particles like lead zirconate titanate (PZT), and barium titanate (BaTiO_3).^{6–10}

Due to the advent of the internet of things (IoT) and Industry 4.0, the interconnectivity required to collect and share the most diverse data requires a large number and variety of sensors. In this sense, piezoelectric composites are promising materials whose applications range from sensors and energy harvesting systems to wearable technology. In order to meet such needs, composites with high moldability, flexibility, and piezoelectric coefficient are highly desirable and, amongst these composites, are the ones based on castor-oil polyurethanes.^{11–14}

Castor oil is attractive to obtain PUR because it has a high number of hydroxyl groups ($-\text{OH}$) that react with isocyanate ($-\text{NCO}$) to form urethane bonds.¹⁵ These hydroxyl groups are derived from ricinoleic acid, which constitutes approximately 80% of the oil. The hydrophobic nature of the triglycerides in castor oil contributes to its excellent mechanical properties, such as the high tensile strength.^{15–17} Castor oil-based polyurethanes are characterized by hard regions (where polymeric chains are oriented) and soft regions (where the chains are random).¹⁵ The concentration of polyol (produced by castor oil) can affect the formation of these regions, as well as the viscosity of the polymer solution and mechanical properties (stiffness and rigidity). When the polyol content is lower than the prepolymer content (isocyanate), there will be fewer soft regions and the polyol/prepolymer solution will be more viscous, which will make the polymer film stiffer and less flexible after polymerization.^{15–17} Therefore, piezoelectric properties of triphasic composites can be directly influenced by the polyol/prepolymer ratio.

In this context, polymer/ceramic composites with connectivity 0–3 have been largely studied due to their easy synthesis.^{18,19} However, one of the problems encountered when evaluating the piezoelectric properties in composites with connectivity 0–3 is the low poling efficiency of the ferroelectric ceramic particles embedded in the polymer matrix.^{20,21} This occurs because the polymer matrix presents low dielectric constant, limiting application under high electric fields, which leads to a low internal electric field on the ceramic particulate. This makes the piezoelectric composite's polarization inefficient and, as a result, influences the piezoelectric response and electromechanical performance.^{20,22}

One alternative to overcoming this problem and increasing the local electric field on the ferroelectric particles in the piezoelectric composite is the addition of a third conductive phase dispersed in the composite matrix, such as conductive particles based on CNTs, graphene,

and conductive polymers.^{23–26} Sudan et al.²⁷ for example, evaluated the effect of aluminum (Al) particles dispersion on the electric, dielectric, and piezoelectric properties of epoxy/PZT composites by analyzing the piezoelectric constant (d_{33}). The authors observed an increase in piezoelectric properties and a rise in dielectric constant for volume fractions of Al less than 0.13 vol.%.

A three-phase piezoelectric composite based on poly(vinylidene fluoride) (PVDF) matrix with PZT, and CB nanoparticles was studied by Li et al.²⁸ They found that the dispersion of CB (0.4 vol.%) in the PZT/PVDF improved both piezoelectric properties and electrical conductivity.²⁸ Similarly, Sanches et al.²⁹ studied the effects of the addition of carbon black nanoparticles on electrical, dielectric, and piezoelectric properties of water-based polyurethane (WPU)/PZT composites. The authors describe synergistic effects between the WPU/PZT/CB composite phases that contributed to the generation of charges between particles, providing better homogeneity of the components and that influenced on WPU crystallization. Furthermore, dispersion of a third conductive phase in the piezoelectric composite with connectivity 0–3 increased the local electric field on the PZT particles. As a result of the difference in electrical conductivity of the two regions at the interface between PZT and conductive regions, charge carriers accumulated in these interfaces, creating a strong local electric field due to the formation of microcapacitors within the composite.²⁹

The present study aims to obtain a three-phase piezoelectric composite composed of a castor oil-based polyurethane matrix, PZT particles and MWCNT, used as fillers. The effects between dispersed phases on the final electrical, dielectric, and piezoelectric properties of the three-phase composites were studied. Specifically, we highlight the synergistic effects found between MWCNT and PZT, which significantly improved the dielectric and electric properties, as well as the piezoelectric coefficient d_{33} of the three-phase composites.

2 | MATERIALS AND METHODS

2.1 | Materials

The following materials were used: bicomponent PUR (pre-polymer (isocyanate) and polyol) was purchased from Sinergia (Araraquara, SP, Brazil) (specific mass equal to 0.96 g/cm^3); non-functionalized MWCNT nanoparticles (specific mass 0.23 g/cm^3) were acquired from CTNano (Center for Technology in Nanomaterials, UFMG, Minas Gerais, Brazil), with purity greater than 95% and approximately 5% of contaminants (Al_2O_3 - Co - Fe); PZT ceramic particles (APC 855), in powder form, were purchased from

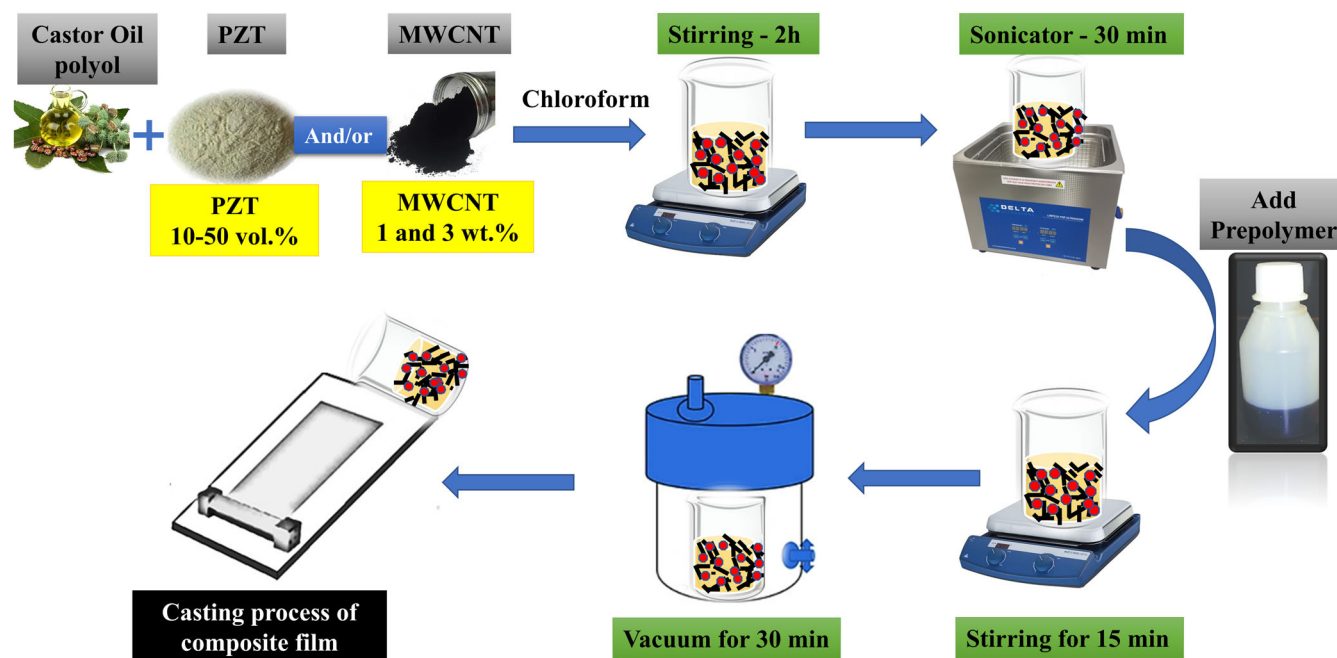


FIGURE 1 A sketch of the method for obtaining biphasic and triphasic piezoelectric composites-based on castor-oil polyurethane. [Color figure can be viewed at [wileyonlinelibrary.com](https://onlinelibrary.wiley.com/doi/10.1002/app.53572)]

American Piezo Ceramics (Mackeyville, PA, USA), whose main characteristics are: $d_{33} \approx 630$ pC/N, piezoelectric voltage constant (g_{33}) $\approx 21 \times 10^{-3}$ Vm/N, relative dielectric constant in 1 kHz ≈ 3300 and $\rho \approx 7.6$ g/cm³. All chemicals were used as received, without any further purification.

2.2 | Preparation of two and three-phase piezoelectric composites

Two and three-phase piezoelectric composite samples with connectivity 0–3 were prepared considering the volumetric fraction of PZT particles in relation to fixed quantities of PUR (3.0 g) according to the Equation (1):

$$m_c = \frac{\rho_c * \vartheta_c}{\rho_p * (1 - \vartheta_c)} * m_p \quad (1)$$

where m_p and ρ_p are mass and specific density of PUR whereas the m_c , $\rho_c * \vartheta_c$ are mass, density, and volumetric fraction of PZT, respectively.

To obtain the two-phase piezoelectric composite 0–3, polyol (2.0 g) and PZT particles at different concentrations (10–50 vol.%) were dispersed in 2.0 ml of chloroform and mixed under constant stirring. After mixing the polyol/PZT/chloroform dispersion for 2 h, the pre-polymer (1.0 g) was added to start the polymerization. Flexible piezoelectric composite films, with thickness ranging from 100 to 250 μ m were

cast from PUR/PZT dispersions onto glass substrates and cross-linked at room temperature for 5 days.

The same route was used to obtain the three-phase piezoelectric composite as shown in Figure 1. PZT particles were added together with MWCNT to the polyol/chloroform mixture and kept for 2 h after adding the prepolymer. To obtain PUR-MWCNT/PZT piezoelectric composite, two quantities of MWCNT (below and above percolation threshold) were used: (i) 1.0 wt.% (4.0 vol.%) and (ii) 3.0 wt.% (7.7 vol.%). The PZT volumetric fractions were the same used to obtain the two-phase composites. Table 1 summarizes the quantity and volumetric fraction of PZT particles, as well as the MWCNT concentration used to prepare these composites. All samples were dispersed with a sonicator for 15 min to improve phase dispersion before pouring onto the glass substrate.

2.3 | Characterization

Scanning electron microscopy (SEM) analysis of the cryo-fractured surfaces of PUR/PZT and PUR-MWCNT/PZT piezoelectric composite films was carried out using an EVO LS15 of Zeiss microscope. All samples were coated with a thin layer of conductive carbon by a sputter coater prior to SEM analysis.

The dc electrical conductivity was measured by the two-probe method using a programmable voltage-current source (Keithley, model 236). Gold electrodes

Samples	MWCNT (wt.%)	PUR/PZT ratio (vol./vol.%)	Amount of PZT (g)
PUR-MWCNT1/ PZT	1.0	90/10	2.41
		80/20	5.43
		70/30	9.31
PUR-MWCNT3/ PZT	3.0	60/40	14.48
		50/50	22.46

TABLE 1 Ratio and quantity of materials used to make the three-phase piezoelectric composites

were evaporated on both faces of the films for electrical contact. The dc electrical conductivity was then calculated using Equation (2):

$$\sigma_{dc} = \frac{1}{R} \frac{L}{A} \quad (2)$$

where R is the resistance obtained from slope of the I versus V graph, A is the electrode area and L is the sample thickness. The dielectric and electrical analysis of PUR/PZT and PUR-MWCNT/PZT piezoelectric composites were performed in the 10^{-2} – 10^6 Hz frequency range at room temperature, using an SI 1260 Solartron Impedance Analyzer with a 1296 Dielectric Interface.

Dielectric and electrical properties may be determined from a set of magnitudes correlated to the Z^* complex impedance formalism, given by the Equation (3):

$$Z^* = Z' + iZ'' \quad (3)$$

where Z' and Z'' are the real and imaginary part of the complex impedance, respectively, and i is the imaginary number. The quantities that can be obtained from Z^* are: (a) complex admittance (Y^*); (b) complex electrical module (M^*); (c) complex dielectric permittivity (ϵ^*); (e) complex electrical conductivity (σ^*). These formalisms are associated to each other, considering the interrelation factor $\mu = i\omega C_0$, where C_0 is the vacuum capacitance, $i(\sqrt{-1})$ the imaginary factor and ω the angular frequency.³⁰

The samples were poled by applying a constant electric field (5.0 MV/m), using a Trek Model 610 C voltage source. The films were polarized in silicone oil using an electric field of 5.0 MV/m with a Trek Model 610C voltage source for 1 h at 60°C and then removed from the silicone oil and with the electric field still applied, while left to cool down to room temperature. The polarization conditions presented correspond to the highest intensity electric field that can be applied without causing electrical rupture of the samples. The d_{33} piezoelectric coefficient was measured by the American Piezo Ceramics (APC) d_{33} Piezo Tester, model 8000. All measurements were performed at 10 different sample locations and their mean values and respective deviations were used in this study.

3 | RESULTS AND DISCUSSION

3.1 | PUR/MWCNT nanocomposite

In the first part of this work, we studied the morphology and electrical properties of PUR/MWCNT nanocomposites used as matrix for the PZT particles. This was necessary to determine MWCNT dispersion in PUR matrix as well as to find the insulator-conductor transition when PUR/MWCNT nanocomposite reaches the percolation threshold.

Figure 2a,b shows the SEM micrographs of neat PUR and PUR/MWCNT nanocomposite containing 3 wt.% MWCNT, respectively. As compared to the neat PUR (Figure 2a), a morphological change in the cryofractured PUR/MWCNT surface can be observed, causing an increase of roughness (Figure 2b). It can also be observed that MWCNT are not evenly distributed throughout the PUR matrix probably due to van der Waals forces between nanotubes and to differences in surface energy of PUR and MWCNT.

The electrical conductivity (σ_{dc}) behavior of PUR/MWCNT nanocomposites as a function of MWCNT concentration is illustrated in Figure 2c. It can be seen that σ_{dc} increases gradually rather than as a sharp percolative insulator-conductor change. This behavior was attributed to polyurethane's molecular structure, which is composed of alternating soft and hard segments.^{29,31,32} The insulator-conductor transition can be observed between 1 and 2 wt.% MWCNT in which σ_{dc} undergoes an abrupt increase from approximately 10^{-12} S/m (100/0) to 10^{-3} S/m (98/02), that is, there was a 9-fold increase in σ_{dc} value of the PUR-MWCNT with 2 wt.% MWCNT addition in relation to neat PUR matrix. To MWCNT concentration greater than the 2 wt.%, the σ_{dc} remains constant.

The σ_{dc} behavior of two-phase composite can be explained by universal percolation theory.^{33,34} Based on this theory, it was possible to calculate the percolation threshold of PUR/MWCNT nanocomposites whose estimated value was 1.57 wt.% MWCNT. According to the percolation theory, the σ_{dc} of a two-phase system can be described by a power law as shown in Equation (4):

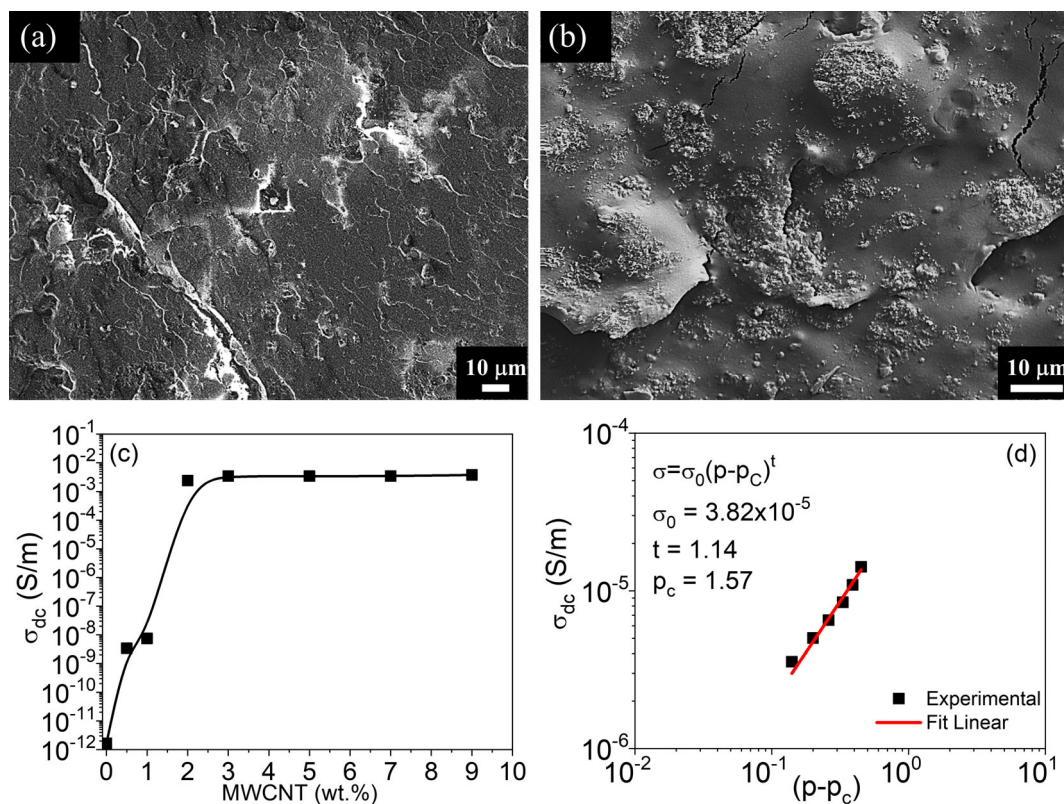


FIGURE 2 Scanning electron microscopy (SEM) images of fractured surface of (a) neat PUR and (b) PUR/MWCNT nanocomposite with 97/3 mass fraction. (c) Graphic of σ_{dc} as a function of mass fraction of MWCNT and (d) fitting of the σ_{dc} as a function of $(p - p_c)$ logarithm graphic. [Color figure can be viewed at wileyonlinelibrary.com]

$$\sigma_{dc} = \sigma_0(p - p_c)^t \quad (4)$$

where p is the volume or mass percentage of the conducting phase, p_c is the critical volume or mass percentage (percolation threshold) at which the insulator to conductor transition occurs, σ_0 is pre-exponential constant and t is the conductivity critical exponent.

The t exponent was determined by fitting σ_{dc} as a function of $(p - p_c)$ as shown in Figure 2d to yield a value of 1.14, which therefore agrees with the classical percolation theory. This result is an indication that the electrical conduction process inside the nanocomposite occurs through a two-dimensional percolation network formed by the MWCNTs.^{35,36}

3.2 | PUR/PZT piezoelectric composite 0–3 without and with MWCNT

3.2.1 | Morphological analysis

Figure 3 shows the SEM images of cryofractured surface of neat PUR, PUR/PZT piezoelectric composite 0–3 and PUR/PZT with 1 wt.% (PUR-MWCNT1/PZT) and 3 wt.% (PUR-MWCNT3/PTZ) MWCNT. The volumetric fraction

of PZT in relation to PUR was equal to 50 vol.% for all piezoelectric samples. It can be seen from Figure 3a,b that PUR surface becomes rougher with the incorporation of PZT (PZT are the brightest regions while PUR-MWCNT/PZT are the darkest ones). The presence of these MWCNT-containing regions may contribute to the increase in local electric field on the PZT particles due to the formation of microcapacitors (in the MWCNT-PZT-MWCNT configuration), that is, they can improve the polarization of PZT particles and, in turn, contribute to the piezoelectric properties of the composites. A similar behavior, that is, a two-phase composite, has also been observed by Nayak for polydimethylsiloxane (PDMS) and PZT.³⁷

Arul et al.³⁸ verified by SEM analysis that the increase in PZT concentration in poly(methyl methacrylate) matrix makes its dispersion more homogeneous, resulting in a greater interaction between particles. Pal et al.³⁹ also verified by SEM that MWCNT dispersion in PVDF/PZT piezoelectric composites improved PZT particle dispersion. Tuff et al.⁴⁰ obtained BaTiO₃-Epoxy-ZnO-based multifunctional composites and observed that larger and more frequent agglomerations of ZnO occurs for higher volume fractions. These agglomerations are attributed to van der Waals forces between

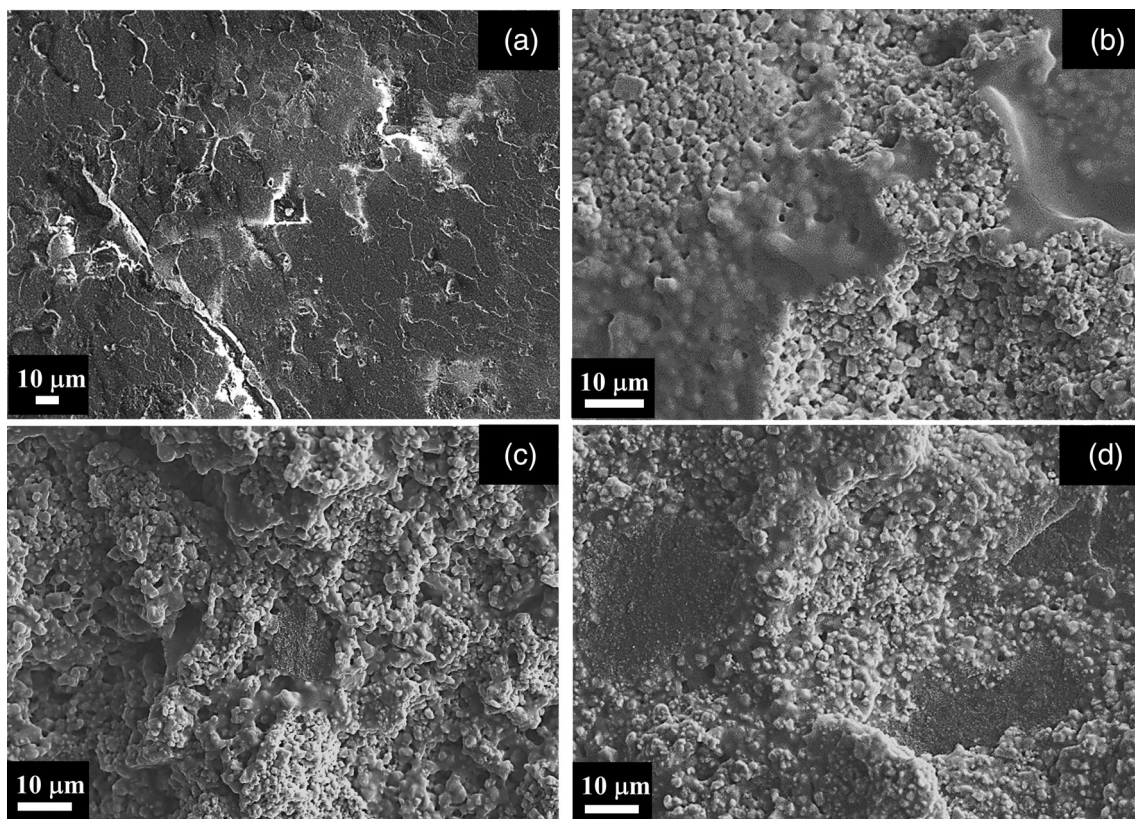


FIGURE 3 Scanning electron microscopy (SEM) analysis of the fractured surface of (a) neat PUR and to piezoelectric composites samples of (b) PUR/PZT, (c) PUR-MWCNT1/PZT and (d) PUR-MWCNT3/PZT all samples with 50 vol.% PZT.

nanoparticles during the solution-based fabrication and the posterior curing of the thin films. In our case, MWCNT agglomeration are caused most probably due to van der Waals forces as well as to an increase in the effective concentration (confinement) of MWCNT in PUR because of the PZT content.⁴¹

3.2.2 | DC electrical analysis

The *dc* electrical analysis was carried out to evaluate the influence of PZT concentration on the *dc* electrical conductivity (σ_{dc}) of the biphasic composite as well as the influence of the addition of a third conductive phase. Figure 4 shows a σ_{dc} plot as a function of the volumetric fraction of PZT. It can be observed that PZT has little influence on the σ_{dc} values of the PUR/PZT piezoelectric composite. This small increase in σ_{dc} can be attributed to the ionic and electronic conduction processes that occur preferentially in PZT grains.^{42,43} On the other hand, MWCNT impacted on the σ_{dc} value of three-phase PUR-MWCNT/PZT piezoelectric composite. For instance, in samples containing 10 vol.% PZT, there was a 5 and 7-fold increase in σ_{dc} values for samples with 1 and 3 wt.% of MWCNT, respectively, when compared to the

PUR/PZT two-phase composite sample with 10 vol.% PZT.

The stronger decrease in σ_{dc} value to piezoelectric composite containing 3 wt.% MWCNT (PUR-MWCNT3/PZT), when PZT concentration increased, can be related to barrier effects that arise by breaking the connectivity of the percolative conduction pathway formed by MWCNT.⁴⁴ For high PZT fractions, free volume is reduced in the matrix, therefore constraining MWCNT to minute polymeric regions and facilitating their interaction through van der Waals bonds, which results in aggregation.⁴³ The increase in PZT concentration also increases the energy barrier that charge carriers must overcome to flow through a material when an electric field is imposed. This breaking of the percolative conduction pathway, in samples whose MWCNT concentration is above the percolation threshold, tends to create conducting regions separated by insulating regions of PZT, thus forming micro-capacitors inside the composite, which may result in a contribution to the poling process of the PZT particles.⁴⁵

On the other hand, samples with 1 wt.% of MWCNT (PUR-MWCNT1/PZT) showed an opposite behavior with respect to the PUR-MWCNT3/PZT samples, that is, when the PZT concentration increased by 10 vol.% there was an

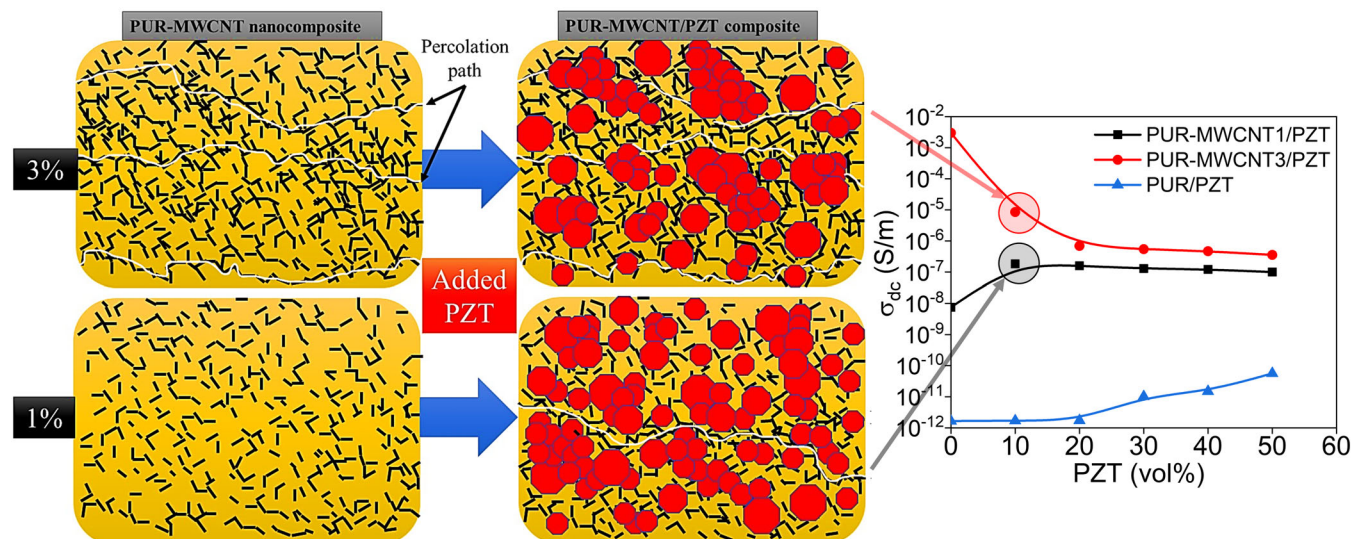


FIGURE 4 A representative sketch illustrating the PZT dispersion effect on the electrical percolation system in PUR-MWCNT/PZT composites. Graphic of σ_{dc} as a function of PZT volumetric fraction introduced into two and three-phase piezoelectric composite. [Color figure can be viewed at wileyonlinelibrary.com]

increase in the σ_{dc} value of the PUR-MWCNT1/PZT three-phase composite. Below the percolation, for lower PZT concentrations, the reduction in free volume of dispersion caused by piezoelectric particles acts to bringing the nanotubes closer together, thus improving the formation of conduction pathways and facilitating the hopping processes.⁴³

Figure 4 shows the possible model of configuration for the three-phasic piezoelectric composite with MWCNT concentration below and above percolation threshold. In the PUR-MWCNT3/PZT composite (MWCNT concentration above the percolation threshold), when the amount of PZT is increased, the percolative electrically conductive path is broken down and the MWCNT tends to form conductive regions. This effect reduces the conductivity of the composite, but, on the other hand, may help its poling process. In samples with MWCNT concentrations lower than the percolation threshold (PUR-MWCNT1/PZT), PZT particles occupy regions in the polymer matrix confining MWCNTs in smaller regions creating conduction channels throughout the sample.²⁹ This effect is seen as increasing the conductivity of the PUR-MWCNT1/PZT composite as showed in the Figure 4.

3.2.3 | Impedance spectroscopy analysis

Figure 5a,c,e shows the real relative dielectric permittivity ($\epsilon'(f)$) as a function of electric field frequency at room temperature for two and three-phase piezoelectric composite with different PZT concentration. For neat PUR, $\epsilon'(f)$ is

nearly independent of frequency. As expected, the $\epsilon'(f)$ value increases with an increase in volume fraction of PZT for the PUR/PZT, PUR-MWCNT1/PZT and PUR-MWCNT3/PZT composites. This gradual increase can be assigned to the high dielectric constant of PZT ceramics in relation to PUR matrix. The $\epsilon'(f)$ magnitude decreased slightly when the ac electric field frequency increased, this frequency-dependent behavior of $\epsilon'(f)$ can be attributed to the reduction in the dielectric constant of PZT particles with increasing frequency, as well as due to space charge interfacial polarization ascribed to the Maxwell-Wagner-Sillars (MWS) effect.^{46,47} This behavior has also been observed by the Riquelme and Raman⁴⁸ in lead-free BZT-BCT/PVDF flexible composites and is attributed to polarization relaxation and interface polarization of space charge, as well as to difficulty of the dipole orientation polarization in the internal structure at the high frequency regime of the piezoelectric composite.⁴⁸

In the low frequency region, $\epsilon'(f)$ of all piezoelectric composite samples increased because of the tendency of dipoles to orient themselves in the direction of an ac electric field. In high frequency region, $\epsilon'(f)$ remains almost constant, that is, the frequency-independent behavior of $\epsilon'(f)$ poses great difficulty to the orientation/rotation of the dipoles in the composite since the periodic reversal of the ac electric field change so fast that no excessive diffusion of charge carrier in its direction occurs, therefore the polarization process caused by charge accumulation is reduced and, as a result, there is a decrease in $\epsilon'(f)$.⁴⁹

The dielectric loss tangent ($\tan \delta$) of the PUR/PZT, PUR-MWCNT1/PZT and PUR-MWCNT3/PZT composites was also evaluated as illustrated in Figure 5b,d,f. It

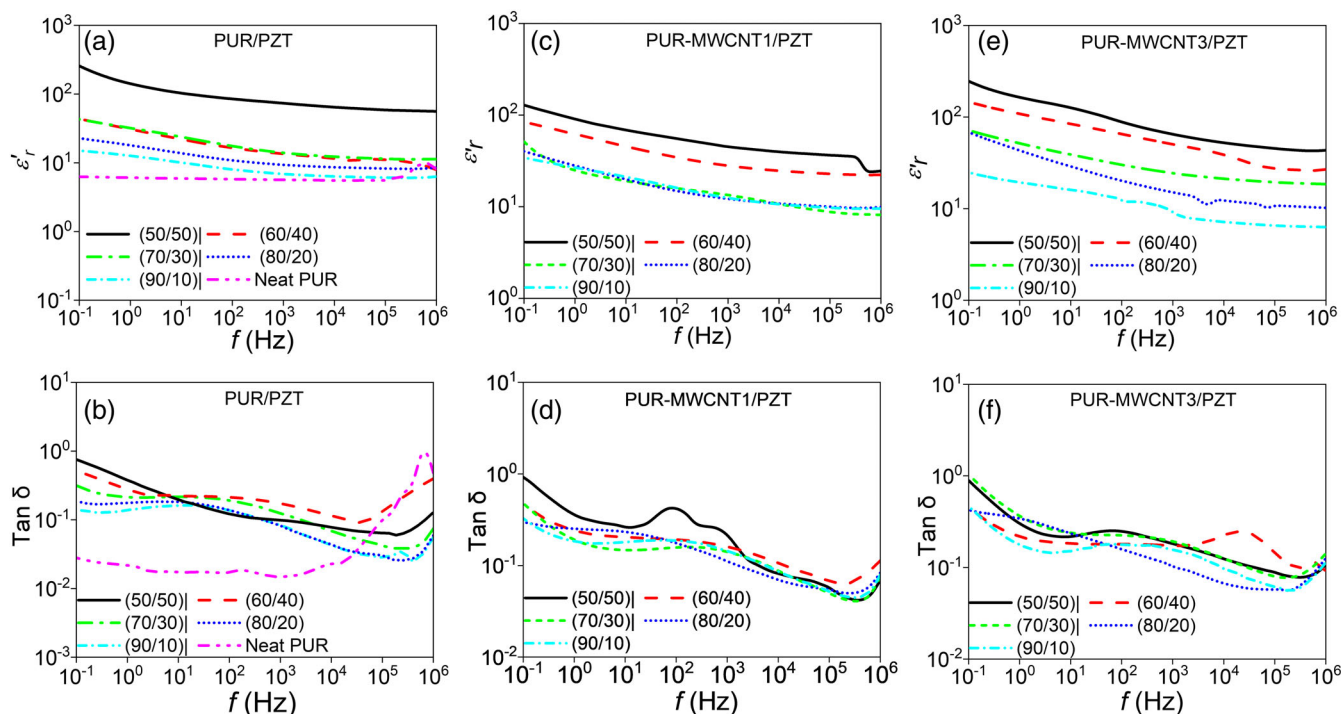


FIGURE 5 Dielectric constant and dielectric loss factor as a function of frequency for the (a–b) PUR/PZT, (c–d) PUR-MWCNT1/PZT and (e–f) PUR-MWCNT3/PZT composites with various PZT volume ratios at room temperature, respectively. [Color figure can be viewed at wileyonlinelibrary.com]

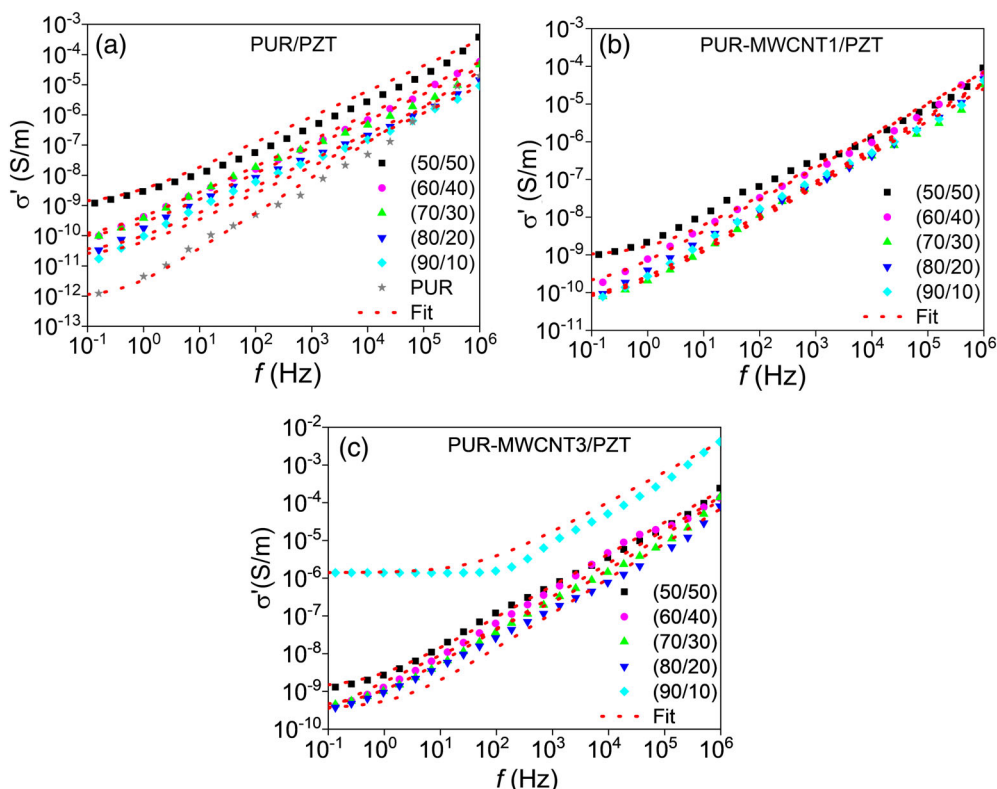


FIGURE 6 Real part of complex electrical conductivity as a function of frequency for the (a–b) PUR/PZT, (c–d) PUR-MWCNT1/PZT and (e–f) PUR-MWCNT3/PZT composites with various PZT volume ratios at room temperature, respectively. [Color figure can be viewed at wileyonlinelibrary.com]

can be observed that $\tan \delta$ increases in comparison with neat PUR when the PZT concentration increased for both samples with and without MWCNT, this behavior can be

attributed principally to the increase of conductivity in the piezoelectric composite samples. The logarithmic form of $\tan \delta$ to two-phase and three-phase piezoelectric

composite decreases with the logarithm of frequency mainly in the low frequency regime. The $\tan \delta$ peak observed in all piezoelectric samples with different PZT concentrations can be attributed to MWS effect and interfacial polarization of space charge, as well as both amorphous dipoles and dipoles at the PZT/amorphous interfaces.^{50,51}

The complex ac electrical conductivity ($\sigma^*(f) = \sigma'(f) + i\sigma''(f)$) analysis is an excellent tool to evaluate the conduction process in different type of materials. Figure 6 shows that the behavior of the real part of ac conductivity $\sigma'(f)$ of samples was analyzed in a wide range of frequencies at room temperature. The $\sigma'(f)$ behavior as function of the frequency for two and three-phase piezoelectric composite with different PZT volumetric concentrations is shown in Figure 6a–c. As expected, all samples present dependent-frequency behavior of $\sigma'(f)$ for the whole frequency range, except for PUR-MWCNT3/PZT with 10 vol.% PZT. This sample has MWCNT concentration above the percolation threshold. Moreover, 10 vol.% PZT dispersion may have broken the percolative conduction pathway of the composite and has large conductive islands where the conduction process occurs when an ac electric field is applied.

It is interesting to point out that the $\sigma'(f)$ behavior for all the samples corroborates with the σ_{dc} value and is influenced by the increase in PZT concentration. It can be also observed in Figure 6, mainly in the low frequency region, that when the PZT concentration increased, $\sigma'(f)$ values also increased for all PUR/PZT, PUR-MWCNT1/PZT and PUR-MWCNT3/PZT composites. Benna et al.⁵² found a similar behavior with respect to $\sigma'(f)$ of the two-phase piezoelectric composite of PVA and BaTiO₃. The authors verified that an increase in BaTiO₃ concentration increased the interfacial polarization, resulting in an increase in composite's conductivity.⁵²

This frequency-dependent behavior of $\sigma'(f)$ in Figure 6 for all PUR/PZT and PUR-MWCNT/PZT composites is characteristic of disordered materials and generally obeys Jonscher's power law according to Equation (5)^{35,53}:

$$\sigma'(f) = \sigma_{dc} + A\omega^n \quad (5)$$

where A is the pre-exponential factor that is related to the strength of polarizability; σ_{dc} is a dc electrical conductivity (plateau or frequency-independent region) and n is the fractional exponent that can vary between 0 and 1.⁵⁴ The n exponent characterizes the interaction degree between the charge carriers and the lattices around them. Values of n range between 0 and 1 and are related to the form through which the conduction mechanism occurs, that is, hopping processes and/or interfacial polarization of space charges.⁵⁵

Fitting Equation (5) from the plot of $\log \sigma'(f)$ versus \log frequency (Figure 6a–c) for all the piezoelectric composites yielded data summarized in Table 2. The n value for the PUR/PZT, PUR-MWCNT1/PZT and PUR-MWCNT3/PZT composite ranged between 0.8 and 1.0, suggesting that the electrical conduction involves hopping process of spatial charges between localized states or spatial charges trapped at the interfaces between the matrix, conductive clusters, and PZT particles in the piezoelectric composites.

3.2.4 | Longitudinal piezoelectric coefficient (d_{33})

Figure 7 shows the comparative analysis of d_{33} piezoelectric coefficient between two and three-phase piezoelectric composites with different PZT concentrations. These results were obtained for all samples poled using an electrical field of 5.0 MV/m at a temperature of 60°C for 1 h.

As expected, for the two-phase PUR/PZT composite, the piezoelectric coefficient d_{33} increases with increasing PZT content. Independent of the ceramic concentration, addition of MWCNT in the two-phase composite promoted a substantial increase in d_{33} .

The polarization process of polymer/ceramic ferroelectric composites is substantially complex and is affected by a number of factors ranging from conductivity of the phases to electrostriction during and after polarization.^{56,57} Ferroelectric ceramics have a high permittivity, compared to polymers, which results in a drastic reduction in the electric field acting on the ceramic grain.^{58,59} This fact generates a discontinuity in the electrical displacement between the polymer/ceramic interface, a fact that, in theory, should make the polarization of the ferroelectric ceramic unfeasible.^{60,61} On the other hand, during the polarization process at high temperatures, spatial charges in the polymeric phase tend to accumulate near the polymer/ceramic interface, increasing substantially the local electric field over the ceramic particulate and removing the discontinuity of the electrical displacement at interfacial regions.^{59,60,62,63} Due to the presence of the third conductive phase, this charge transport can be facilitated by both altering the permittivity and bulk conductivity of the material and reducing the migration time of the charges.⁶⁴ In addition, the third conductive phase allows the formation of microcapacitive systems with the ceramic acting in a possible intensification of the local field as observed by measurements of the d_{33} coefficient. The PUR-MWCNT1/PZT (90/10), PUR-MWCNT3/PZT (90/10) and PUR-MWCNT3/PZT (80/20) composites were not able to be polarized due to their high conductivity.

Samples	σ_{dc} (S/m)	A	n
Neat PUR	9.72×10^{-13}	2.53×10^{-12}	1.17
PUR/PZT (90/10)	2.06×10^{-11}	4.25×10^{-10}	0.89
PUR/PZT (80/20)	2.69×10^{-11}	7.45×10^{-10}	0.87
PUR/PZT (70/30)	7.45×10^{-11}	2.06×10^{-10}	0.87
PUR/PZT (60/40)	7.19×10^{-11}	3.68×10^{-10}	0.86
PUR/PZT (50/50)	1.07×10^{-11}	2.51×10^{-9}	0.84
PUR-MWCNT1/PZT (90/10)	6.23×10^{-11}	1.64×10^{-10}	0.89
PUR-MWCNT1/PZT (80/20)	6.62×10^{-11}	2.10×10^{-10}	0.87
PUR-MWCNT1/PZT (70/30)	6.70×10^{-11}	1.58×10^{-10}	0.87
PUR-MWCNT1/PZT (60/40)	1.34×10^{-10}	5.88×10^{-10}	0.84
PUR-MWCNT1/PZT (50/50)	9.40×10^{-10}	1.18×10^{-9}	0.82
PUR-MWCNT3/PZT (90/10)	1.40×10^{-6}	6.24×10^{-8}	0.80
PUR-MWCNT3/PZT (80/20)	3.56×10^{-10}	1.98×10^{-10}	0.90
PUR-MWCNT3/PZT (70/30)	3.11×10^{-10}	3.48×10^{-10}	0.90
PUR-MWCNT3/PZT (60/40)	3.74×10^{-10}	7.38×10^{-10}	0.87
PUR-MWCNT3/PZT (50/50)	1.21×10^{-9}	1.92×10^{-9}	0.83

TABLE 2 Parameters obtained from Fitting theoretical–experimental adjustments using Jonscher's equation for PUR/PZT, PUR-MWCNT1/PZT and PUR-MWCNT3/PZT composite samples and neat PUR

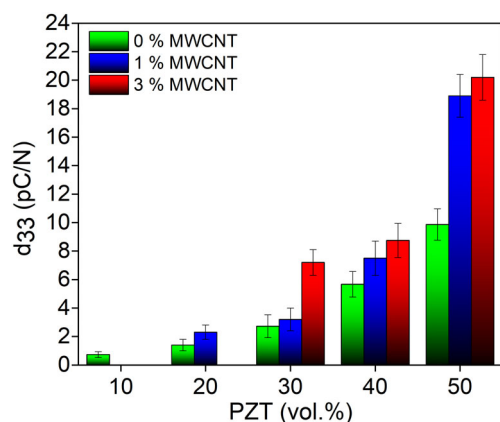


FIGURE 7 Comparative measurements of d_{33} coefficient measured for 30 days after poling for PUR/PZT, PUR-MWCNT1/PZT and PUR-MWCNT3/PZT piezoelectric composite samples as the function of PZT concentration. [Color figure can be viewed at wileyonlinelibrary.com]

A comparative analysis of the d_{33} coefficient results between two- and three-phase piezoelectric composites (1 and 3 wt.% of MWCNT) with different volume concentrations of PZT was also performed. Figure 7 shows a gradual increase in the d_{33} coefficient of the piezoelectric composite for both MWCNT conductive phase (at different PZT concentrations) in comparison with the two-phase composite. Similar results are observed in the literature when carbon-based nanofiller are used as the third conductive phase in piezoelectric composites.^{29,39,65} Tang et al.⁶⁶ found a similar behavior for the PVDF/PZT piezoelectric composite by varying the mass proportion

of graphene. The authors observed that the increase in mass concentration of graphene up to 0.6 wt.% increased d_{33} due to an increase in the dielectric strength of the PVDF matrix caused by graphene, which resulted in intensifying the poling process of PZT particles. For composites whose graphene concentration is higher than 0.6 wt.%, there was a decrease in d_{33} due to a greater dielectric loss.⁶⁶ Our best results were obtained with three-phase piezoelectric composites containing 3 wt.% MWCNT.

Unlike the two-phase PUR/PZT composite, some samples of the three-phase piezoelectric composite could not be polarized, especially for 10 and 20 vol.% PZT. This behavior may be related to increased electrical conductivity of matrix because of the MWCNT phase and the low concentration of PZT particles.

4 | CONCLUSIONS

PUR/PZT and PUR-MWCNT/PZT piezoelectric composite films with different PZT (10–50 vol.%) and MWCNT concentrations, below and above of percolation threshold, were prepared by casting. Addition of MWCNT helped enhance the dielectric constant, electrical conductivity, and piezoelectric performance of composites. The decrease in dc conductivity with increasing PZT concentration, for three-phase composites containing 3 wt.% MWCNT was attributed to the breaking of the conductive percolation pathway. On the other hand, for the three-phase composites containing 1 wt.% MWCNT, there was

an increase in electrical conductivity which was attributed to the creation of a conductive pathway resulting from the increase in the effective concentration of MWCNT in PUR. Moreover, dielectric analysis showed a gradual increase in $\varepsilon'(f)$ to all piezoelectric composite due to the high dielectric constant of PZT particles in relation to PUR matrix. However, $\varepsilon'(f)$ presented a frequency-dependent behavior that can be attributed to the reduction in the dielectric constant of PZT particles with increasing frequency, as well as to space charge interfacial polarization ascribed to the Maxwell–Wagner–Sillars effect. As expected, all samples had a frequency-dependent behavior of $\sigma'(f)$ in the range between 10^{-1} and 10^6 Hz, which is characteristic of disordered materials and generally obeys Jonscher's power law. The n exponent value for PUR/PZT, PUR-MWCNT1/PZT and PUR-MWCNT3/PZT ranged between 0.8 and 1.0, suggesting that the electrical conduction involves hopping processes of spatial charges between localized states and/or spatial charges trapped at the interfaces between the PUR matrix, conductive clusters and PZT particles the piezoelectric composite. Comparative analysis of the d_{33} piezoelectric coefficient between PUR/PZT and PUR-MWCNT/PZT piezoelectric three-phase nanocomposites showed a significant increase when the MWCNT conductive phase was added, which can be attributed to the formation of microcapacitors due the development of conductive regions improving PZT particle polarization.

AUTHOR CONTRIBUTIONS

Michael J. Silva: Conceptualization (lead); data curation (equal); formal analysis (equal); funding acquisition (lead); investigation (equal); methodology (equal); project administration (lead); resources (equal); supervision (lead); validation (equal); visualization (equal); writing – original draft (equal); writing – review and editing (equal). **Fernando C. M. Freire Filho:** Conceptualization (equal); data curation (lead); formal analysis (lead); investigation (equal); methodology (equal). **Josiane A. Santos:** Conceptualization (equal); data curation (equal); formal analysis (equal); investigation (equal); methodology (equal). **Alex O. Sanches:** Conceptualization (equal); formal analysis (equal); methodology (equal); validation (equal); visualization (equal); writing – original draft (equal); writing – review and editing (equal). **Eliton S. Medeiros:** Data curation (equal); formal analysis (equal); investigation (equal); validation (equal); writing – original draft (equal); writing – review and editing (equal). **José A. Malmonge:** Conceptualization (equal); data curation (equal); formal analysis (equal); methodology (equal); validation (equal); writing – original draft (equal); writing – review and editing (equal).

ACKNOWLEDGMENTS

The authors are grateful to the Sao Paulo State Funding Agency (FAPESP) (grant 2017/19809-5 and CEPID – CDMF Grant 2013/07296-2), and Conselho Nacional de Desenvolvimento Científico e Tecnológico-CNPq (Grant 158889/2019-2), for their financial support and scholarship.

DATA AVAILABILITY STATEMENT

The data that support the findings of this study are available on request from the corresponding author. The data are not publicly available due to privacy or ethical restrictions.

ORCID

Alex O. Sanches  <https://orcid.org/0000-0003-2730-7435>

Eliton S. Medeiros  <https://orcid.org/0000-0002-9033-9141>

José A. Malmonge  <https://orcid.org/0000-0002-1773-3142>

Michael J. Silva  <https://orcid.org/0000-0002-2971-1696>

REFERENCES

- [1] P. Costa, J. Oliveira, L. Horta-Romaris, M.-J. Abad, J. A. Moreira, I. Zapirain, M. Aguado, S. Galván, S. Lanceros-Mendez, *Compos. Sci. Technol.* **2018**, *168*, 353.
- [2] D. Rajak, D. Pagar, P. Menezes, E. Linul, *Polymers (Basel)* **2019**, *11*, 1667.
- [3] N. Chamankar, R. Khajavi, A. A. Yousefi, A. Rashidi, F. Golestanifard, *Ceram. Int.* **2020**, *46*, 19669.
- [4] A. K. Ghosh, M. Dwivedi, *Processability of Polymeric Composites*, New Delhi, Springer India **2020**, p. 29.
- [5] I. O. Oladele, T. F. Omotosho, A. A. Adediran, *Int. J. Polym. Sci.* **2020**, *2020*, 1.
- [6] T. Liu, J. Pei, J. Xu, Q. Guo, R. Li, *Mater Res Express* **2019**, *6*, 066303.
- [7] Y. Li, X. Huang, L. Zeng, R. Li, H. Tian, X. Fu, Y. Wang, W.-H. Zhong, *J. Mater. Sci.* **2019**, *54*, 1036.
- [8] J. Dong, C. Jia, M. Wang, X. Fang, H. Wei, H. Xie, T. Zhang, J. He, Z. Jiang, Y. Huang, *Compos. Sci. Technol.* **2017**, *149*, 75.
- [9] J. Defebvin, S. Barrau, J. Lyskawa, P. Woisel, J. M. Lefebvre, *Compos. Sci. Technol.* **2017**, *147*, 16.
- [10] J. G. L. Costa, P. H. F. Rodrigues, L. L. Paim, A. O. Sanches, J. A. Malmonge, M. J. da Silva, *Mater. Res.* **2020**, *23*, 1.
- [11] Y. Zhang, C. K. Jeong, J. Wang, H. Sun, F. Li, G. Zhang, L.-Q. Chen, S. Zhang, W. Chen, Q. Wang, *Nano Energy* **2018**, *50*, 35.
- [12] S. Mishra, L. Unnikrishnan, S. K. Nayak, S. Mohanty, *Macromol. Mater. Eng.* **2019**, *304*, 1800463.
- [13] S. P. Muduli, S. Parida, S. K. Behura, S. Rajput, S. K. Rout, S. Sareen, *Polym. Adv. Technol.* **2022**, *33*, 3628.
- [14] M. Habib, I. Lantgios, K. Hornbostel, *J. Phys. D. Appl. Phys.* **2022**, *55*, 423002.
- [15] F. C. Alves, V. F. dos Santos, F. M. Monticeli, H. Ornaghi, H. da S. Barud, D. R. Mulinari, *Polym. Polym. Compos.* **2021**, *29*, S1063.
- [16] A. Sardari, A. A. Sabbagh Alvani, S. Ghaffarian, *R. Prog. Org. Coat.* **2019**, *133*, 198.

- [17] P. Saha, C. Khomlaem, H. Aloui, B. S. Kim, *Polymers (Basel)* **2021**, *13*, 1387.
- [18] R. L. B. de Freitas, W. K. Sakamoto, L. P. S. Freitas, F. Castro, A. P. Lima Filho, C. Kitano, A. A. de Carvalho, *IEEE Sens. J.* **2018**, *18*, 5067.
- [19] C. K. Wong, F. G. Shin, *Frontiers of Ferroelectricity: A Special Issue J. Mater. Sci.* **2006**, *41*, 229.
- [20] G. de Campos Fuzari, M. O. Orlandi, E. Longo, W. L. D. B. Melo, W. K. Sakamoto, *Smart Mater. Struct.* **2013**, *27*, 11733.
- [21] M. T. Sebastian, H. Jantunen, *Int. J. Appl. Ceram. Technol.* **2010**, *7*, 415.
- [22] X. F. Liu, C. X. Xiong, H. J. Sun, L. J. Dong, R. Li, Y. Liu, *Mater. Sci. Eng. B Solid State Mater. Adv. Technol.* **2006**, *127*, 261.
- [23] S. Aboubakr, A. Hajjaji, M. Rguiti, K. Benkhouja, C. Courtois, *Int. J. Hydrog. Energy* **2017**, *42*, 19504.
- [24] Y. Shen, Y. Guan, Y. Hu, Y. Lei, Y. Song, Y. Lin, C.-W. Nan, *Appl. Phys. Lett.* **2013**, *103*, 072906.
- [25] G. Petrossian, N. Aliheidari, A. Ameli, *J. Compos. Sci.* **2020**, *4*, 137.
- [26] H. J. Kim, Y. J. Kim, *Mater. Des.* **2018**, *151*, 133.
- [27] U. Sundar, K. A. Cook-Chennault, S. Banerjee, E. Refour, *J. Vacuum Sci. Technol. B Nanotechnol. Microelect.: Mater. Proc. Measur. Phenom.* **2016**, *34*, 041232.
- [28] R. Li, Q. Guo, Z. Shi, J. Pei, *Ferroelectrics* **2018**, *526*, 176.
- [29] A. O. Sanches, D. H. F. Kanda, L. F. Malmonge, M. J. da Silva, W. K. Sakamoto, J. A. Malmonge, *Polym. Test.* **2017**, *60*, 253.
- [30] R. Simoes, J. Silva, S. Lanceros-Mendez, R. Vaia, *J. Mater. Sci.* **2010**, *45*, 268.
- [31] M. J. D. Silva, D. H. F. Kanda, H. N. Nagashima, *J. Non-Cryst. Solids* **2012**, *358*, 270.
- [32] E. Segal, R. Tchoudakov, M. Narkis, A. Siegmann, *Polym. Eng. Sci.* **2002**, *42*, 2430.
- [33] M. J. Silva, A. O. Sanches, C. R. Cena, H. N. Nagashima, E. S. Medeiros, J. A. Malmonge, *Polym. Compos.* **2021**, *42*, 1519.
- [34] L. S. Cardoso, G. E. Gonçalves, D. H. F. Kanda, R. F. Bianchi, H. N. Nagashima, *Appl. Phys. A Mater. Sci. Process* **2017**, *123*, 799.
- [35] P. V. Rebeque, M. J. Silva, C. R. Cena, H. N. Nagashima, J. A. Malmonge, D. H. F. Kanda, *Polym. Compos.* **2019**, *40*, 7.
- [36] M. Mazaheri, J. Payandehpeyman, S. Jamasb, *Appl. Compos. Mater.* **2022**, *29*, 695.
- [37] S. Nayak, D. Khastgir, *J. Appl. Polym. Sci.* **2019**, *136*, 47307.
- [38] K. T. Arul, M. S. R. Rao, *J. Phys. Chem. Solids* **2020**, *146*, 109371.
- [39] A. Pal, A. Sasmal, B. Manoj, D. P. Rao, A. K. Haldar, S. Sen, *Mater. Chem. Phys.* **2020**, *244*, 122639.
- [40] W. Tuff, P. Manghera, J. Tilghman, E. van Fossen, S. Chowdhury, S. Ahmed, S. Banerjee, *J. Electron. Mater.* **2019**, *48*, 4987.
- [41] T. Kaur, A. Thirugnanam, *RSC Adv.* **2016**, *6*, 39982.
- [42] B. Boukamp, M. Pham, D. Blank, H. Bouwmeester, *Solid State Ionics* **2004**, *170*, 239.
- [43] A. O. Sanches, M. J. Silva, L. F. Malmonge, N. R. S. Basso, J. A. Malmonge, *J. Appl. Polym. Sci.* **2021**, *138*, 50865.
- [44] Z. Wang, T. Wang, M. Fang, C. Wang, Y. Xiao, Y. Pu, *Compos. Sci. Technol.* **2017**, *146*, 139.
- [45] G. Wang, *ACS Appl. Mater. Interfaces* **2010**, *2*, 1290.
- [46] S. Moharana, M. K. Mishra, B. Behera, R. N. Mahaling, *Polym. Sci. Ser. A* **2017**, *59*, 405.
- [47] W. Wu, X. Huang, S. Li, P. Jiang, T. Toshikatsu, *J. Phys. Chem. C* **2012**, *116*, 24887.
- [48] S. A. Riquelme, K. Ramam, *Mater Res Express* **2019**, *6*, 116331.
- [49] M. K. Mishra, S. Moharana, B. Behera, R. N. Mahaling, *Front. Mater. Sci.* **2017**, *11*, 82.
- [50] S. A. Riquelme, K. Ramam, A. F. Jaramillo, *Results Phys.* **2019**, *15*, 102800.
- [51] P. Thomas, K. T. Varughese, K. Dwarakanath, K. B. R. Varma, *Compos. Sci. Technol.* **2010**, *70*, 539.
- [52] P. Beena, H. Jayanna, *Polym. Polym. Compos.* **2019**, *27*, 619.
- [53] B. M. Greenhoe, M. K. Hassan, J. S. Wiggins, K. A. Mauritz, *J. Polym. Sci. B Polym. Phys.* **1918**, *2016*, 54.
- [54] A. Dhahri, E. Dhahri, E. K. Hlil, *RSC Adv.* **2018**, *8*, 9103.
- [55] M. Jouni, J. Faure-Vincent, P. Fedorko, D. Djurado, G. Boiteux, V. Massardier, *Carbon NY* **2014**, *76*, 10.
- [56] K. S. Lam, Y. Zhou, Y. W. Wong, F. G. Shin, *J. Appl. Phys.* **2005**, *97*, 104112.
- [57] K. S. Lam, Y. W. Wong, L. S. Tai, Y. M. Poon, F. G. Shin, *J. Appl. Phys.* **2004**, *96*, 3896.
- [58] Z. M. Dang, J. K. Yuan, J. W. Zha, T. Zhou, S. T. Li, G. H. Hu, *Prog. Mater. Sci.* **2012**, *57*, 660.
- [59] C. K. Wong, F. G. Shin, *J. Appl. Phys.* **2005**, *97*, 034111.
- [60] G. Eberle, H. Schmidt, W. Eisenmenger, *IEEE Trans. Dielectr. Electr. Insul.* **1996**, *3*, 624.
- [61] T. Furukawa, *IEEE Trans. Electr. Insul.* **1989**, *24*, 375.
- [62] T. Furukawa, K. Ishida, E. Fukada, *J. Appl. Phys.* **1979**, *50*, 4904.
- [63] W. Eisenmenger, M. Haardt, *Solid State Commun.* **1982**, *41*, 917.
- [64] W. K. Sakamoto, E. de Souza, D. K. Das-Gupta, *Mater. Res.* **2001**, *4*, 201.
- [65] H. Kim, J. Johnson, L. A. Chavez, C. A. Garcia Rosales, T.-L. B. Tseng, Y. Lin, *Ceram. Int.* **2018**, *44*, 9037.
- [66] J. Tang, J. Liu, H. Huang, *J. Electron. Mater.* **2019**, *48*, 4033.

How to cite this article: F. C. M. Freire Filho, J. A. Santos, A. O. Sanches, E. S. Medeiros, J. A. Malmonge, M. J. Silva, *J. Appl. Polym. Sci.* **2023**, *140*(9), e53572. <https://doi.org/10.1002/app.53572>